water

MDPI

*Article*

# Testing Utility of ICESat-2 and SWOT Altimetry in Monitoring Monthly Groundwater Levels of Dune Field Water Table Lakes

**Nawaraj Shrestha [1,*], Troy E. Gilmore [1,2], Aaron R. Mittelstet [2] and R. Matthew Joeckel [1]**

[1] Conservation Survey Division, School of Natural Resources, University of Nebraska-Lincoln, Lincoln, NE 68583, USA; gilmore@unl.edu (T.E.G.); rjoeckel3@unl.edu (R.M.J.)
[2] Biological Systems Engineering Department, University of Nebraska-Lincoln, Lincoln, NE 68583, USA; amittelstet2@unl.edu
* Correspondence: nshrestha3@unl.edu

## Abstract

Groundwater levels are usually mapped as water table contours produced from point data, that is, hydraulic heads measured in modest numbers of observation wells distributed across a given region. The typically sparse distributions of wells, especially in remote areas, severely limit the number of observations that can be made and may lead to ambiguous groundwater-level estimates at unsampled locations. Satellite altimetry provides reliable estimates of hydraulic heads wherever surface water and groundwater intersect, regardless of how remote the location is. Therefore, we tested the use of Ice, Cloud, and Land Elevation Satellite 2 (ICESat-2) and Surface Water and Ocean Topography (SWOT) measurements of water levels in interdune water table lakes to characterize groundwater levels in the Nebraska Sandhills (central USA), the largest dune field in the Western Hemisphere. Our satellite altimetry estimates of groundwater levels in the Nebraska Sandhills closely approximate the measurements made in nearby observation wells. ICESat-2 showed a root-mean squared error (RMSE) of 0.68 m with ±0.45 m standard deviation (SD). SWOT estimated an RMSE of 0.75 m with ±0.76 m SD. Monthly groundwater levels were estimated using kriging with an external drift and generalized additive models, with RMSEs ranging from 1.9 m to 3.3 m and with unbiased errors (mean error of −0.003 m to 0.153 m). We conclude that satellite altimetry has potential for the remote measurements of groundwater levels under certain geographic conditions, especially where groundwater-dominated lakes are prevalent.

**Keywords:** satellite altimetry; remote sensing; Nebraska Sandhills; lake groundwater level; kriging; generalized additive model

Check for updates

Academic Editor: Chang Huang

Received: 15 May 2026
Revised: 29 June 2026
Accepted: 30 June 2026
Published: 1 July 2026

**Copyright:** © 2026 by the authors. Licensee MDPI, Basel, Switzerland. This article is an open access article distributed under the terms and conditions of the Creative Commons Attribution (CC BY) license.

## 1. Introduction

Groundwater comprises about 30% of global freshwater resources. It supplies one-third of all freshwater usage, or 36%, 42% and 27% of domestic, agricultural, and industrial consumption, respectively [1]. Groundwater sustains baseflow to many rivers, lakes, and wetlands during periods of minimal or no rainfall. Nevertheless, groundwater is sparsely measured and monitored, primarily through observation wells, which are costly to install, maintain, and repeatedly sample [2]. Sparse observations inhibit our ability to characterize groundwater recharge, discharge, flow, storage, and distribution. Furthermore, climate change and other anthropogenic impacts are expected to alter the global water cycle and groundwater hydrology, producing effects such as increased groundwater flooding

(e.g., Mittelstet [3]). Groundwater recharge may be reduced by 10–20% in the future, although groundwater use could increase as climate variability spurs escalating demands and population growth [4,5]. Better quantification of groundwater levels will be essential for the sustainable development of society and the maintenance of global ecosystems.

Satellite sensors can advance groundwater quantification and provide novel insights into groundwater systems. Satellite altimetry is already widely used to estimate the relative height of the water surface in streams, lakes and reservoirs [6]. Altimeters such as ICESat-2 (Ice, Cloud, and Land Elevation Satellite) and Surface Water and Ocean Topography (SWOT) provide continuous observations with reasonable estimates of water surface elevation throughout the year. ICESat-2, a satellite-based light detection and ranging (LiDAR) system equipped with a high-resolution photon-counting laser altimeter, provides lake water-level retrievals with unprecedented accuracy with a root mean square error (RMSE) of 0.06–0.5 m. SWOT employs a Ka-band radar interferometer (KaRIn) at 35.75 GHz to measure ocean surface topography and inland water elevations, including lakes, reservoirs, rivers and wetlands [7]. SWOT estimates lake water levels with an average bias of $-0.01 \pm 0.13$ m and a mean absolute error (MAE) of less than 0.1 m when validated against ICESat-2 data [8]. The median unbiased RMSE of SWOT vs. gauge is 0.53 m, and the median Pearson's correlation coefficient is 0.91 [9]. Studies using satellite altimetry have vastly improved the monitoring and understanding of inland water dynamics, especially those of large lakes, reservoirs, rivers, and wetlands. However, fewer studies use altimetry to measure the water levels of smaller and shallower groundwater-dependent ecosystems. Our study combines the greater spatial and temporal coverage of SWOT with precise measurements from ICESat-2 to provide unprecedented detail of hitherto sparsely measured groundwater levels at a regional scale [10]. In doing so, we vastly improve the understanding of water dynamics in a large and important ecoregion, the Nebraska Sandhills (hereafter Sandhills).

The 4700 groundwater-fed lakes in the Sandhills lie below the level of the regional potentiometric surface and are areas of focused groundwater discharge [11]. Changes in the water levels and areas of these lakes are important indicators of regional climate and environmental effects, including fluctuations in groundwater [12]. Improved characterization of water-level fluctuations can assist in identifying the effects of climate and management practices in one of the most important recharge areas of the subcontinental-scale High Plains aquifer system [13]. In addition, much of the Sandhills is remote, and land is chiefly under private ownership, hampering long-term, large-scale in situ monitoring. Satellite altimetry, however, provides reliable estimates of lake levels that can be used to approximate groundwater levels. Shrestha [14] demonstrated the utility of aerial infrared LiDAR and the waterline method to estimate the water levels in lakes in the Sandhills and to approximate the level of the unconfined aquifer. The results showed potential for further development and refinement. Groundwater levels estimated in this manner can then be predicted at unsampled locations using geostatistical methods. Geostatistics provides unbiased estimates of groundwater-level variation and the uncertainty associated with it. Using the spatial correlation structure derived from sampled locations, geostatistics can predict water levels at unsampled locations. Methods such as ordinary kriging (OK), universal kriging (UK), kriging with an external drift (KED), and co-kriging are extensively used to map groundwater levels [15–17]. However, kriging assumes a linear relationship between a response and explanatory variables, and this relationship may not hold true in many natural processes, which mostly obey curvilinear functions [18]. Generalized additive models (GAMs), a semiparametric form of generalized linear models (GLM), automatically derive model parameters directly from data, allowing flexibility in the modeling of response variables. GAMs use a combination of linear and nonlinear components to reveal hidden patterns in data. Although GAM is widely applied in environmental, climate, and

ecological modeling, it is less commonly used in groundwater-level mapping [19–21]. For example, Asquith [22] used GAM to interpolate and extend monthly groundwater levels of individual wells in the Mississippi River Valley alluvial aquifer in the south-central USA. However, the unique combination of a voluminous regional aquifer, a relatively shallow water table, widely distributed lakes, and frequent satellite (ICESat-2 and SWOT) observations provides an exceptional opportunity to remotely assess monthly groundwater levels in the Sandhills.

The widespread distribution of lakes in the Sandhills provides an opportunity to measure and estimate groundwater levels from lake levels on a monthly basis. Current studies mostly use observations from individual wells to model groundwater-level changes and their distribution [23]. However, a relatively small number of sparsely distributed wells in the Sandhills cannot characterize the spatial and temporal variability of groundwater levels and the associated uncertainty. Spatially and temporally explicit knowledge and understanding of groundwater are necessary for proper management and decision-making for sustainable management of scarce groundwater. We formulate a novel approach that integrates satellite altimetry, lake water level, and statistics to estimate monthly groundwater levels. Our hypothesis is to test whether lake water levels derived from satellite altimetry (ICESat-2 and SWOT) serve as reliable proxies for groundwater level. Our specific objectives are to (i) estimate groundwater levels using lake water level at a monthly scale using satellite altimetry and (ii) evaluate kriging and generalized additive models to characterize the groundwater level variation.

## 2. Materials and Methods

### *2.1. Study Area*

The Sandhills are the largest sand dune field in the Western Hemisphere, covering approximately 50,000 km$^2$ [24] (Figure 1). The climate of the Sandhills is characterized by high evapotranspiration, with annual reference crop evapotranspiration ($ET_0$) ranging from 1285 mm to 1667 mm [13] and comparatively low annual precipitation ranging from 430 mm in the west to 610 mm in the east. The mean temperature ranges between ~−14 °C in January and ~31 °C in July, and the mean annual temperature is 8.4 °C. Despite its subhumid to semiarid climate, the Sandhills host hundreds of interdunal lakes, more than 2000 km$^2$ of wetlands, and many perennial streams (Figure 1) [25,26]. Most Sandhills lakes do not have surface inlets or outlets, and their levels are generally lower than the regional potentiometric surface, as is typical for groundwater-fed lakes, indicating that they act as areas of focused groundwater discharge [11,27]. The majority (>76%) of the lakes are smaller than 0.2 km$^2$ but some are larger than 2 km$^2$ (<1%) [14]. The larger lakes are chiefly in the western part of the Sandhills, and streams dammed by dune migration in the early Holocene Epoch, between 6000 and 12,000 years ago, produced some of them [26]. Most Sandhills lakes are also generally shallow, having an overall mean depth of ~0.8 m. Therefore, they are seasonally or annually dynamic [28]. Regional topography slopes gently from west to east, but local topography is highly variable due to the existence of various types of large, complex dunes. Irrigation is limited in the Sandhills, and there is a high groundwater recharge rate (~13% of precipitation) relative to many arid and semiarid regions [27,29].

### *2.2. Data Sources and Processing*

Multiple datasets were utilized to evaluate the potential of the altimeters to estimate groundwater levels. These are (a) along-track heights (ATL08) from ICESat-2, (b) SWOT Single-Pass Lake water levels, (c) groundwater levels from observation wells, and (d) monthly lake area boundaries from Sentinel-2.

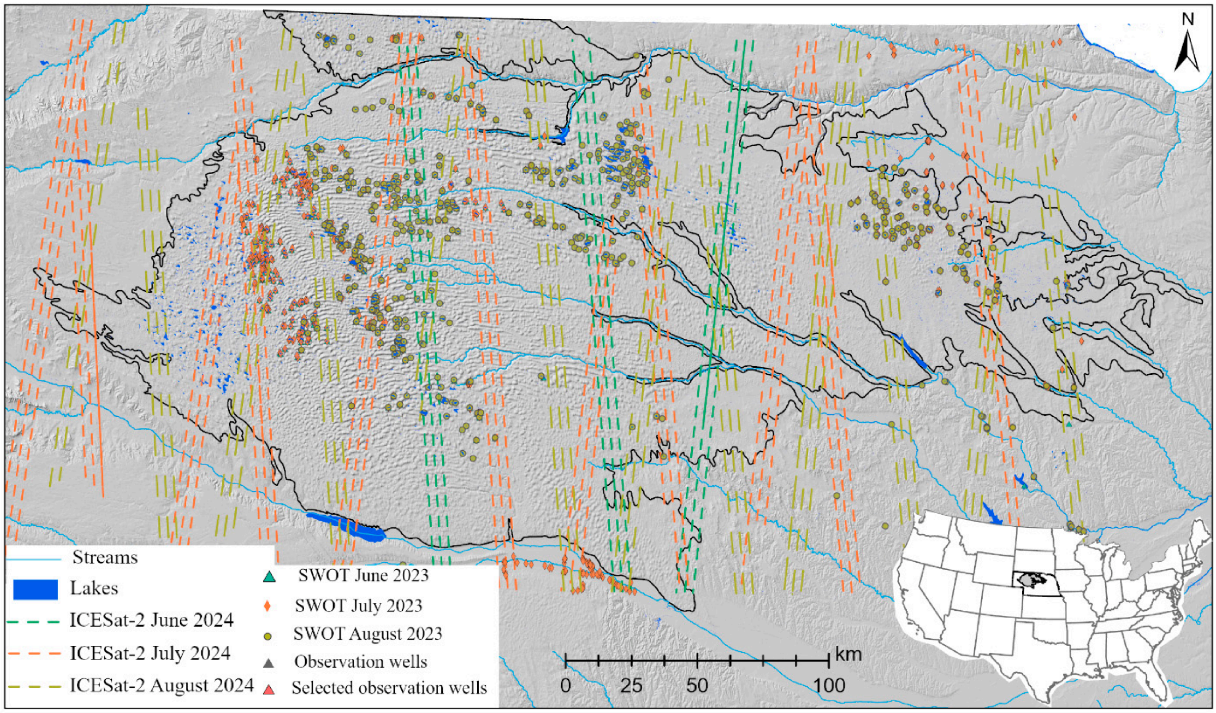



**Figure 1.** Distribution of lakes, satellite altimetry observations, and observation wells in the Nebraska Sandhills (Sandhills). ICESat-2 samples the central Sandhills during June and most of the Sandhills during July and August. SWOT samples cover most of the Sandhill lakes for each of the months considered for the study period. Therefore, a combination of ICESat-2 and SWOT enables monthly lake water level measurements and subsequent groundwater levels in the Sandhills. We selected observation wells near lakes and underlying unconfined aquifers to validate our estimations made from lake water levels.

#### 2.2.1. Sentinel-2

We used Sentinel-2 satellite image archives to delineate the boundary between lake and land surface areas. Sentinel-2, a constellation of Sentinel-2a and Sentinel-2b satellites, has a spatial resolution of 10, 20, and 60 m with 13 spectral bands in the visible, near-infrared, and shortwave infrared regions. The revisit frequency of each single satellite is 10 days, and the combined constellation revisit is 5 days. The level 2A images used in this study are bottom-of-atmosphere reflectances that are corrected for radiometric, geometric, and atmospheric effects (e.g., atmospheric scattering, aerosol particles, and water vapor) [30].

#### 2.2.2. ICESAt-2 ATL08

The ICESat-2, launched in September 2018, uses the Advanced Topographic Laser Altimeter System (ATLAS) and produces six beams at a pulse rate of 10 kHz at 532 nm. Each beam has a 3 m diameter footprint on the ground and is arranged in three pairs, separated by 3.3 km in the across-track direction. The strong and weak beams of each pair are separated by two 90 m footprints of approximately 14 m in diameter, with a separation distance of 0.70 m between the footprints along the track direction [31]. ICESat-2 revisits the same geographic location in a 91-day repeat cycle.

We used the ALT08 land/water vegetation elevation product to estimate terrain and canopy height along the track of the satellite. The ATL08 terrain and canopy heights are provided at a fixed step size of 100 m along the ground track, which is referred to as a segment. We used the terrain best-fit height (h_te_best_fit), which is the terrain elevation at the mid-point location of each 20 m segment. The mid-segment terrain elevation is determined by selecting the best of three fits (linear, third-order, and fourth-order poly-

nomials) to the terrain photons along a 100 m segment [31]. We filtered ICESat-2 ATL08 observations using a terrain quality score greater than 85, where a score near 100 indicates a high-quality estimate of the terrain height. We also used uncertainty of ground height estimates (h_te_uncertainty), which includes all known uncertainties such as geolocation, pointing angle, timing, and radial orbit errors. To compare with the other data sets, we converted the reference ellipsoid height to orthometric height (NAVD88) using the Vertical Datum transformation tool (VDatum) developed by NOAA (available at https://vdatum.noaa.gov/welcome.html (accessed on 14 May 2026)).

#### 2.2.3. SWOT L2 Water Surface Elevation

The SWOT satellite mission was launched in December 2022, led by the Centre National d'Études Spatiales (CNES) and the National Aeronautics and Space Administration (NASA). The KaRIn instrument measures water surface elevation (WSE) within two 50 km-wide swaths, separated by a 20 km wide nadir gap [10]. KaRIn uses a High Rate mode at a fine spatial resolution (∼5 m × 10–70 m) to measure terrestrial water features (e.g., lakes and rivers). SWOT operates in a 21-day repeat with an average global revisit time of 11 days [32]. Importantly, SWOT can monitor small lakes with an area as small as 0.0625 $km^2$. Thus, it monitors features that were too small to be observed by previous nadir satellite altimetry missions.

We used SWOT Level 2 Lake Single-Pass Vector Data Product (SWOT_L2_HR_LakeSP_D) to measure surface water measurements for lakes and unclassified water bodies. The product reports water surface elevation, surface area, and quality indicators for each observed lake using polygons generated from the PIXCVec pixel cloud. It includes features linked to the Prior Lake Database, as well as unassigned features not recognized as lakes or rivers in the Prior Lake Database or Prior River Database [33]. The SWOT WSE employs the EGM2008 geoid model, and it also corrects for media delays (e.g., wet and dry troposphere, ionosphere), crossover discrepancies, and tidal effects (solid, load, and pole tides) to ensure consistency in the WSE measurements. We converted the EGM2008 geoid model to NAVD88 using the Vertical Datum transformation tool (VDatum) developed by NOAA (available at https://vdatum.noaa.gov/welcome.html). Additionally, we filtered the lake WSE for total uncertainty (wse_u), the random-only component of the uncertainty (wse_r_u), and the standard deviation of the WSE of all the pixels composing the lake (wse_std). We also used a quality flag (quality_f = 0), the fraction of the lake's total area covered by dark water (dark_frac < 0.5) and cross-over calibration (xovr_cal_q = 0) to reduce uncertainty in lake-water measurements. Here, dark water refers to the backscatter of the radar signal from the water surface rather than the product of dissolved organic matter.

#### 2.2.4. Observation Wells

We used hourly depth-to-water observation-well data collected and archived by the Conservation and Survey Division in the School of Natural Resources at the University of Nebraska-Lincoln. These data have been checked for quality and consistency [23]. The depth to water was then subtracted from the surveyed land surface elevation to obtain the local elevation of the water table. We used corresponding water levels that matched the date and time (or nearest time) of ICESat-2 and SWOT observations (see Tables S1 and S2 in Supplement) from a total of nine observation wells distributed throughout the Sandhills (Figure 1). The number of wells used varied depending on the corresponding data availability between the satellite altimeters and observation wells.

### *2.3. Method*

#### 2.3.1. Monthly Lake Boundary Extraction

We filtered Sentinel-2 images with cloud cover less than 20% and used FMASK to mask out any remaining clouds in Google Earth Engine (GEE). A monthly mosaic was created using a median filter in the Sandhills. A random forest classifier was applied to extract the boundaries of lakes. B2 (Blue), B3 (Green), B4 (Red), B8 (NIR), B5, B6, B7 (Red Edge), B8A (Narrow NIR), and B11, B12 (SWIR) bands were chosen as predictor variables (Figure 2). The random forest classifier uses an ensemble of decision trees to minimize variance in "noisy" data, reduce overfitting of predictions and provide higher accuracy. It is widely used in processing remotely sensed imagery, and particularly in the classification of water and wetlands [34,35]. A random forest classifier requires substantially smaller labeled datasets and lower computational resources than methods such as deep learning. Training samples (~25,000 pixels as training and ~11,000 pixels as testing) were generated iteratively to have high-quality classified maps as labeled by human interpreters. We used a default parameter of 50 trees because increasing the number of trees does not necessarily increase classification results [36]. Validation of lake boundaries was carried out using independent random samples (100 samples per month) generated and labeled using a combination of Google Earth and National Agricultural Imagery Program (NAIP) images for corresponding months. The monthly lake boundaries were projected, and smaller polygons that did not represent water bodies were removed. We also removed polygons with areas of less than 0.008 $km^2$ to reduce the effect of smaller misclassified pixels in ephemeral water around lakes and wetlands [12]. The smaller polygons were also removed to avoid the effect of clustering and overfitting the variogram [37]. Similarly, any triangular and irregular-shaped polygons were removed using the perimeter-to-area ratio [12].

#### 2.3.2. Lake Water Level Estimation

The monthly lake boundary was used to summarize the ICESat-2 water levels. We used the minimum, mean, maximum, and standard deviation to summarize the water levels within each overlapping lake polygon. With smaller and shallower lakes in the Sandhills, any lake water levels with standard deviations of greater than 0.99 were considered outliers and removed from further analysis. Small lakes typically had the same minimum, maximum, and mean elevation values, so they were eliminated from the analysis. Other lakes that produced abnormally large minimum, maximum, and mean values—interpreted as artifacts of sensor and processing errors—were also eliminated. These preliminary data cleaning processes reduce uncertainty and provide manageable data volume during analysis. The lake water levels that remained after this quality-control process were then converted to points for geostatistical analysis. We calculated the average lake water level (hereafter, lake groundwater level-LGL) for lakes with multiple observations within the corresponding months. We used 292, 299, 336, and 142 LGLs for the four growing-season months of May, June, July, and August of 2023.

#### 2.3.3. Validation of Lake Groundwater Level

The LGLs derived from ICESat-2 and SWOT were validated against the water levels measured in the nine observation wells. Timeseries observations from the wells were compared with the corresponding LGLs estimated using ICESat-2 and SWOT. We used a total of 33 observations for ICESat-2 and 28 observations for SWOT to validate water levels (see Tables S1 and S2 in Supplement). Observation wells that are nearest to the lakes and underlying the unconfined aquifer were selected for comparison. We also corrected LGL for the ambient hydraulic gradient difference due to separation distance and groundwater flow gradient [14]. This correction allows a comparison between LGL

and observation wells on the same equipotential surface. A correction factor was added to the LGL if the lake was below the elevation of the observation well, but the correction factor was subtracted from the LGL if the lake was above the elevation of the observation well. The correction factor is estimated as the product between distance and the gradient between the lake and observation well (see calculations in Supplement Tables S1 and S2). We estimated the mean error, standard deviation (SD), root mean squared error (RMSE) and bootstrap analysis (5000 iterations) of ME to compare LGL, corrected LGL and observation well (see Figure 2).

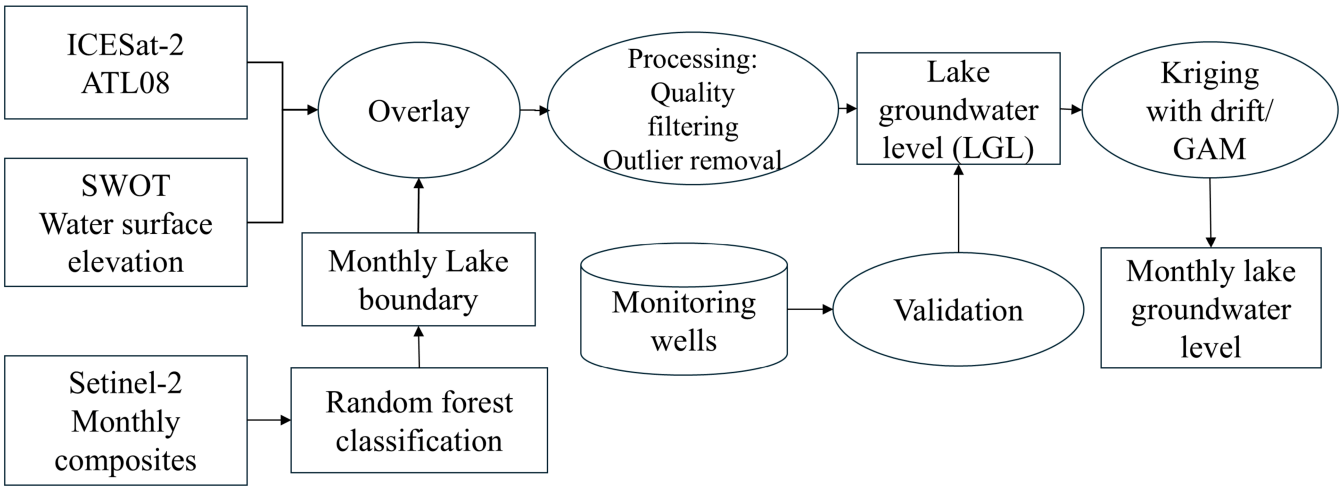



**Figure 2.** Workflow to compute monthly lake groundwater level (LGL) using satellite altimetry, kriging with an external drift, and a generalized additive model. Rectangular shapes indicate data/output, oval shapes indicate major process and database.

#### 2.3.4. Geostatistical Estimation and Prediction

We used geostatistics to estimate and predict the monthly LGLs in Sandhills. Geostatistics uses the sampled attribute ($Z$) at location $s_i$ to estimate the ($Z$) at the unsampled location $s_0$. The observation is decomposed into the mean and the stochastic component (random variable). In the UK, the mean or the trend component is estimated using polynomial functions, while KED uses auxiliary information such as elevation as a trend component [37,38]. We used a semivariogram to determine the spatial dependence of the stochastic component using residuals at unsampled locations. We experimented with multiple kriging approaches and found that KED provided better accuracy than OK and UK. We therefore used KED for further analysis. Kriging methods and their variants are detailed by Desbarats [38].

#### 2.3.5. Kriging with an External Drift

We used a digital terrain model (DTM) to estimate the drift present in the groundwater level. A coefficient of determination estimated using regression indicated a strong association ($R^2 > 0.95$) between the LGL and the terrain elevation values. We also determined the optimal resolution for KED at 90, 200, 500, 700, and 1000 m grids. A higher-resolution grid (<90 m) overwhelmed prediction with local topographic variation, resulting in noisy estimates of groundwater levels, while coarser-resolution grids (>500 m) averaged the groundwater level of the entire area of interest. Therefore, we selected a 200 m grid as the optimal resolution for KED. We used a residual sum of squares (RSS) to evaluate theoretical models. The model with the least RSS was used to determine the spatial correlation. The semivariogram does not indicate the presence of a trend, while directional variograms were used to remove the presence of anisotropy after the drift is removed (see Figure S1 in Supplementary Materials).

2.3.6. Generalized Additive Models

GAMs are a semiparametric approach suitable to model complex nonlinear patterns. GAMs are a response variable using an additive combination of various parametric terms and smooth functions of predictor variables. The smooth function provides advantage over linear regression and other similar methods. The general form of GAM is

$$y_i = \mathrm{X}_i\Theta + f(x_i) + \cdots + \varepsilon_i \quad (1)$$

where $y_i$ is the response variable, $\beta_0$ is an intercept, $\mathrm{X}_i$ is a matrix with parametric and suitably transformed predictor variables, $\Theta$ is a parametric matrix, $f$ is the smoothing function, and $\varepsilon_i$ are errors that are independent and identically distributed with zero mean.

The $\mathrm{X}_i\Theta$ is parametric regression component of GAM. In this study $y_i$ is the LGL, $x_i$ is the numerical representation of latitude and longitude for LGL observations. GAM fits using penalized iterative least squares and a generalized cross-validation score for the smoothness control on the smooth functions [39].

We used multiple combinations of gam using the mgcv package version 1.9-4 (see Supplement Table for models). Our evaluation suggested that the model without smoothing of elevation provided the best predicted surface. We therefore used the following form of GAM in our study.

$$\mathrm{LGL}_{\mathrm{GAM}} = \mathrm{gam}(\mathrm{y} \sim \mathrm{s}(\mathrm{E}, \mathrm{N}) + \log(\mathrm{elevation})) \quad (2)$$

We determined the optimal model of characterizing the predictor variable using Akaike Information Criterion (AIC) and generalized cross-validation (GCV) (see Table S3 in Supplement). We selected the model with the lowest AIC and GCV values along with higher degrees of freedom. Models with smoothing function for individual coordinates in Easting and Northing resulted in lower AIC and GCV. Similarly, adding terrain elevation as a smooth function resulted in higher AIC and GCV. Therefore, we used a model with combined coordinates in the smoothing function. To ensure that the model captured any non-linear patterns in the data for each month, we started the model with a minimum basis dimension (k) of three to minimize over-fitting. The basis dimension defines the maximum complexity that a smooth term can achieve and therefore controls the upper limit of its effective degrees of freedom (EDF). We used GAM diagnostic checks, including the k-index and *p*-value, to determine whether the selected basis dimension was sufficient to capture the underlying patterns in the data. If the k-index and *p*-values for a model were low, we increased the basis dimension by increments of one until the model fit stabilized. A model was considered stabilized when the k-index was near to one and there was a non-significant *p*-value (see Supplement Table S4). The final basis dimension was selected as the smallest value that adequately represented the observed nonlinear patterns while avoiding unnecessary model complexity [39]. We also evaluated model validity using histograms and Q-Q plots (see Supplement Figure S2), Breusch–Pagan test and Moran's I statistics.

2.3.7. Validation of Interpolated Surfaces

We used k-fold (10-fold) cross-validation to determine the accuracy of the predicted LGL surface. The method divides the data into subsets. One subset is used to test while the others are used to predict. We used mean error, mean absolute error (MAE), mean square error (MSE), and RMSE to evaluate the accuracy of the predicted surface. MSE is sensitive to outliers as it measures the magnitude of error, while RMSE provides a standard deviation of the residuals. We used the residual sum of squares (RSS) to evaluate the goodness-of-fit between the empirical and theoretical variogram models.

The accuracy of the extracted lake area was validated using the overall user (i.e., correctness) and producer (i.e., sensitivity) accuracies. The samples were generated randomly and labeled using visual image interpretation of NAIP images. We compared the GAM and KED using the Wilcoxon signed-rank test across cross-validation folds along with bootstrap confidence intervals. Bootstrap resampling (5000 iterations) was used to estimate confidence intervals of the root mean squared error difference.

## 3. Results

### *3.1. Accuracy of Lake Areas and Lake Groundwater Levels*

The monthly lake area, with an overall accuracy greater than 95% and an error of commission less than 5% and an error of omission less than 8%, showed accurate delineation of the boundary between the lake and land surface area.

Our results indicate that lake water level closely estimates field-measured groundwater levels in the Sandhills. The ICESat-2 estimates are within 0.68 m RMSE ± 0.45 m SD, while SWOT water level estimates are within 0.75 m RMSE ± 0.76 m SD (see Tables S1 and S2 in supplement). A linear plot between the observation wells and LGLs (corrected for ambient hydraulic gradient) (Figure 3) shows a high correspondence with $R^2$ greater than 99%. A bootstrap analysis of mean error (bias) of uncorrected LGL indicates substantial positive (3.51 m; 95% CI: −0.075 to 7.389 m) and negative bias (−6.45; 95% CI: −8.714 to −4.037 m) for ICESat-2 and SWOT, respectively. An ambient hydraulic gradient-corrected LGL indicates negative bias (−0.563; −0.697 to −0.427 CI) for ICESat-2 and no significant bias (−0.034; −0.309 to 0.241 CI) for SWOT. These results demonstrate that correction for ambient hydraulic gradient substantially reduces systematic error. The results suggest that the LGL-derived data using satellite altimeters provides sufficient accuracy to characterize monthly groundwater levels.

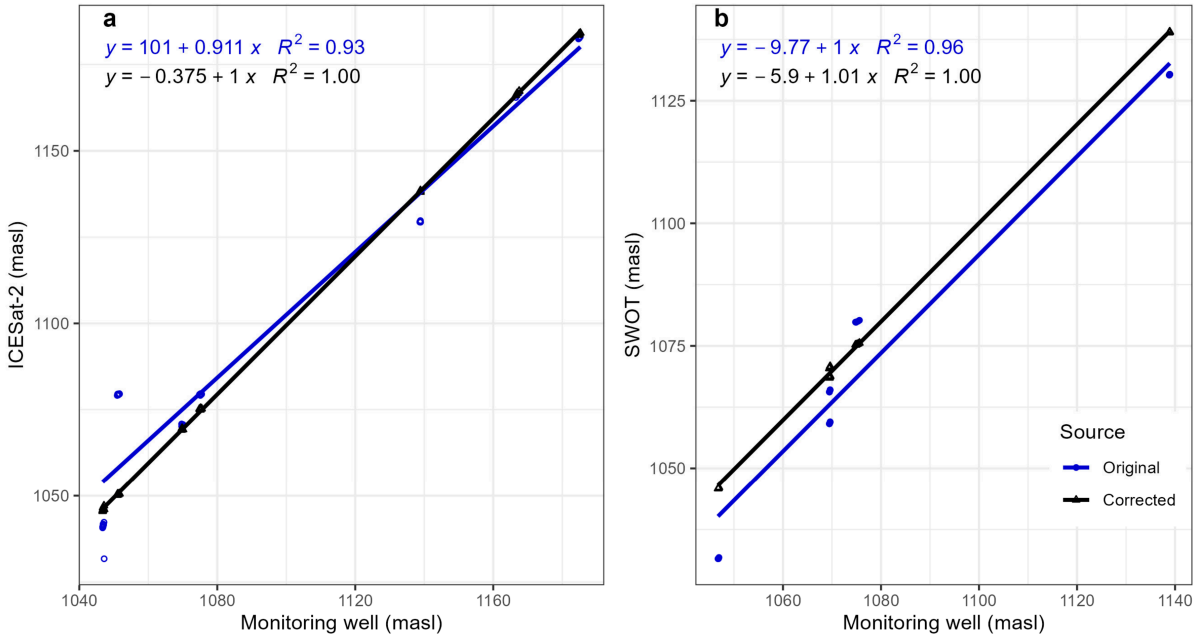



**Figure 3.** A comparison plot between the ICESat-2 (**a**) and SWOT (**b**) water level estimates in the Sandhills indicates high correlation and correspondence. Blue points are uncorrected LGLs, and black points are corrected for ambient hydraulic gradients between lakes and observation wells.

### *3.2. Spatial Dependence on Groundwater Level*

A semivariogram analysis of monthly LGL showed that spherical, Gaussian, and Matern (Ste) variogram models resulted in the best-fit variograms for different months (see Supplement Figure S1). Table 1 reports the best-fitting variogram models and their parameters. May, June, July, and August exhibit the low RSS, but the range varied depending on the month. A nugget-to-sill ratio of less than 0.75 for May, June, and July indicates moderate to high spatial dependence, whereas greater values for July indicate weak dependence. A variable has strong dependence if the nugget-to-sill ratio is less than 0.25, moderate dependence if values are between 0.25 and 0.75, and weak dependence if values are greater than 0.75 [40].

**Table 1.** Comparison of theoretical variogram model parameters using kriging with an external drift for May, June, July, and August in 2023.

| Variogram Parameters | May-23 | Jun-23 | July-23 | August-23 |
|---|---|---|---|---|
| **Best Model** | Gaussian | Spherical | Sph | Ste |
| **Nugget** | 4.4 | 4.3 | 4.7 | 7.8 |
| **Sill** | 6.4 | 5.9 | 5.9 | 81 |
| **Nugget/Sill** | 0.68 | 0.73 | 0.79 | 0.09 |
| **Range** | 7829 | 46,299 | 93,833 | 80,656 |
| **RSS** | $6.1 \times 10^{-6}$ | $1.38 \times 10^{-5}$ | $5.64 \times 10^{-6}$ | $6.06 \times 10^{-5}$ |
| **Kappa** | - | - | | 10 |

Results from GAMs on residual histograms and Q-Q plots showed that the residuals did not substantially deviate from a normal distribution. *p*-values greater than 0.05 for all study months in the Breusch–Pagan test indicate no evidence of heteroscedasticity. Negative Moran's value for all months showed an absence of positive spatial autocorrelation in the residuals and suggested that the spatial smooth terms effectively accounted for the spatial structure in the data (see Supplement Table S4).

### *3.3. Groundwater Level Prediction*

Cross-validation results show that the monthly LGL maps were unbiased with mean error estimates close to zero. May, June, and August showed similar distribution of error values, while July showed higher errors. The quality of prediction not only depends on the number but also the distribution of sample (LGL) observations. A lower number of observations (e.g., August) resulted in higher errors, while a larger number of observations distributed throughout the study area (e.g., June) resulted in lower errors. However, a higher number of observations (e.g., May), clustered in the western Sandhills, resulted in higher errors. A comparison between GAM and KED indicates that GAM estimates are better for most of the months (Table 2).

**Table 2.** A cross-validation comparison between May, June, July, and August using kriging with an external drift (KED) and generalized additive model (GAM). Square brackets indicate the number of LGL observations; all units are in m.

| Month/Error Metrics | Mean Error | | MAE | | MSE | | RMSE | |
|---|---|---|---|---|---|---|---|---|
| | KED | GAM | KED | GAM | KED | GAM | KED | GAM |
| May (292) | 0.040 | 0.008 | 1.670 | 1.537 | 5.854 | 5.505 | 2.419 | 2.346 |
| June (299) | 0.010 | −0.008 | 1.569 | 1.399 | 4.409 | 3.914 | 2.100 | 1.978 |
| July (336) | −0.006 | −0.006 | 2.138 | 1.538 | 7.308 | 4.321 | 2.703 | 2.079 |
| August (142) | 0.051 | −0.181 | 1.777 | 1.754 | 5.445 | 6.361 | 2.333 | 2.522 |

The paired Wilcoxon signed-rank tests showed significant differences between GAM and KED prediction errors in May, June, July, and August ($p < 0.05$). Bootstrap resampling of the paired error differences (GAMs − KED) indicated that the 95% confidence intervals did not overlap zero, showing better prediction for all months by GAM than KED (Table 3).

**Table 3.** Comparison of predictive performance between GAM and KED models based on paired Wilcoxon signed-rank tests and bootstrap confidence intervals of prediction error differences (GAM-KED).

| Month | V Statistic | *p*-Value | Median Difference | 95% CI |
|---|---|---|---|---|
| May | 16,410 | $5.66 \times 10^{-4}$ | 0.134 | 0.006–0.255 |
| June | 16,481 | $7.12 \times 10^{-5}$ | 0.17 | 0.068–0.270 |
| July | 15,769 | $1.97 \times 10^{-12}$ | 0.6 | 0.447–0.756 |
| August | 3383 | $5.65 \times 10^{-4}$ | 0.431 | 0.156–0.710 |

### *3.4. Spatial and Temporal Distribution of Lake Groundwater Levels*

The predicted LGL maps using KED and GAM showed the spatial and temporal variability among May, June, July, and August of 2023. The western Sandhills, which have more lakes and subsequently a larger number of observations, showed accurate representation of groundwater levels, while eastern and southeastern Sandhills with a smaller number of lakes showed higher uncertainty in the groundwater level. The predicted maps using the KED and GAM showed similar patterns in groundwater elevation. The contour generated using maps of the predicted LGL indicates the difference in prediction lies in the areas with sparse water level observations (see Figure S3 in Supplement).

While the predicted surface reveals similar patterns in both KED and GAM, considerable differences are observed in the error surfaces (Figures 4 and 5). KED has resulted in smoother error surfaces than the GAMs (Figure 4). The magnitude of error varied between 2 and 4 m for KED (Figure 4), although the magnitude of error varied between 0.30 and 4 m for GAMs. GAMs resulted in low errors for interdune valley bottom areas (~40 cm) and significantly higher errors in adjacent sand dunes (~2–3 m) (Figure 5). This result indicates that GAMs provide better estimates of the local water level variation, while KED characterizes regional patterns in the Sandhills.

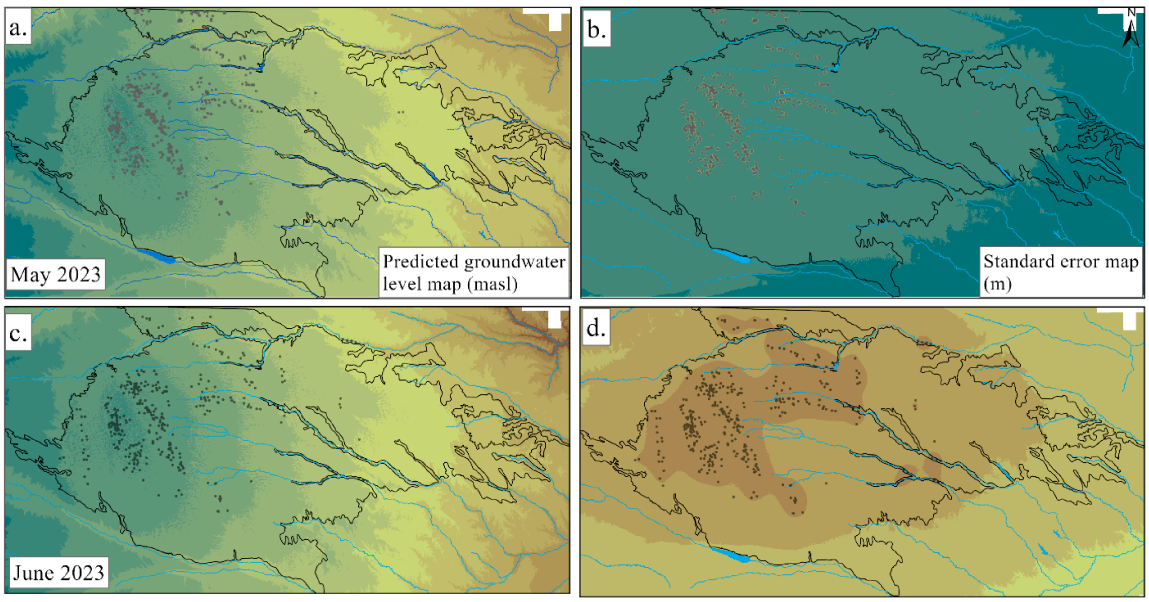



**Figure 4.** *Cont.*

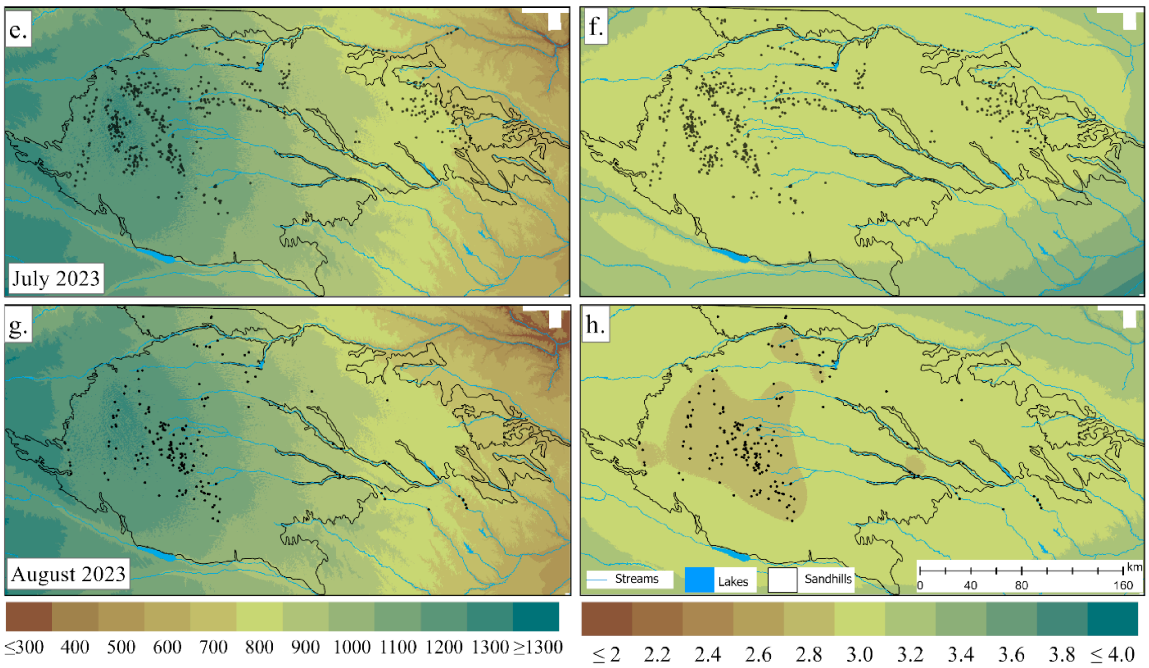



**Figure 4.** Monthly groundwater level maps estimated using kriging with an external drift in the Nebraska Sandhills. The left panels (**a**,**c**,**e**,**g**) show the predicted groundwater level (masl) while the right panels (**b**,**d**,**f**,**h**) show the standard error (m) associated with the corresponding months.

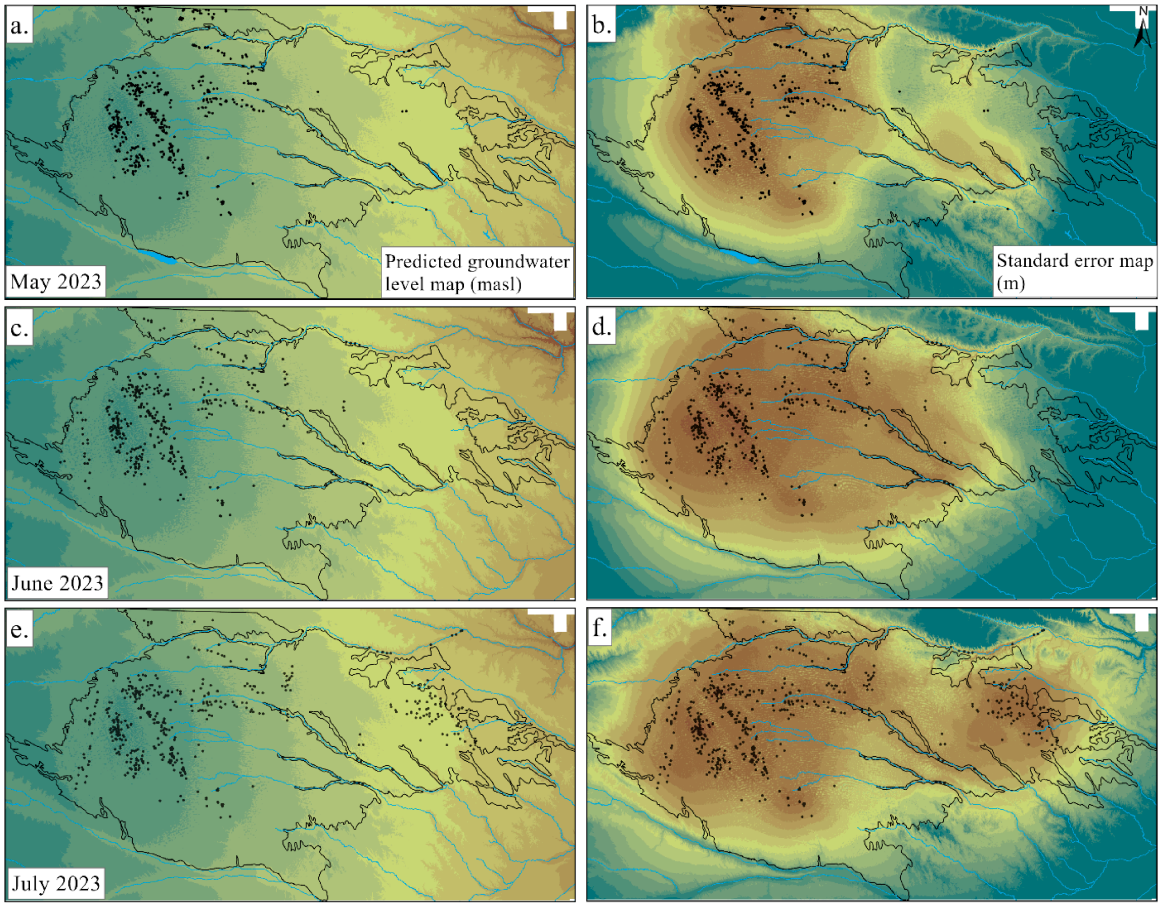



**Figure 5.** *Cont.*

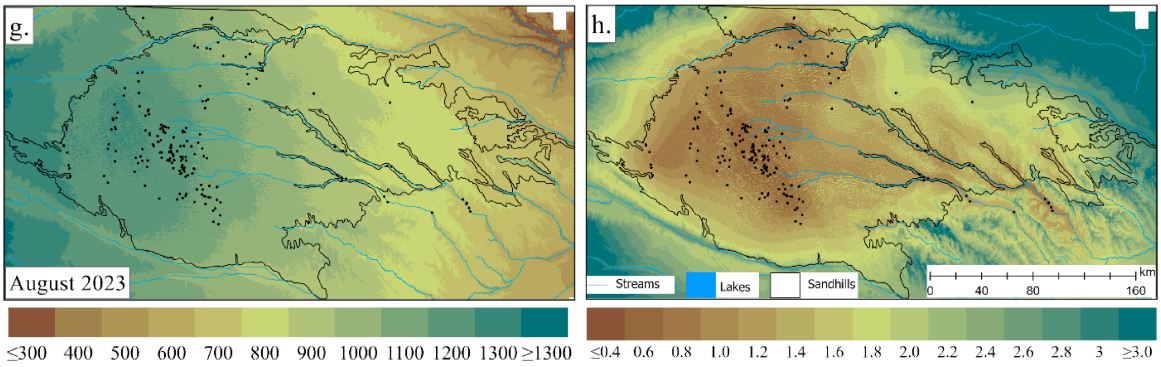



**Figure 5.** Monthly groundwater level maps estimated using a generalized additive model (GAM) in the Nebraska Sandhills. Maps on the left side (**a**,**c**,**e**,**g**) show the predicted groundwater level (masl) while the corresponding maps on the right (**b**,**d**,**f**,**h**) show the standard error (m) associated with the corresponding months.

Similarly, our results in standard error reveal that the accuracy of the map of predicted LGL largely depends on the number and distribution of sample observations. A well-distributed sample observation results in higher accuracy with lower uncertainty (Figures 4c–f and 5c–f) while a smaller number of observations with limited spatial distribution results in higher uncertainty (Figures 4g,h and 5g,h). Similarly, clustered observations result in higher uncertainty than the well-distributed observations in the monthly groundwater level (Figures 4a,b and 5a,b).

## 4. Discussion

Lakes in the Sandhills are areas of focused groundwater discharge, and our method assumes that the lake water level in the Sandhills represents the groundwater level. Results from validation show that the lake water level represents the groundwater level. However, lake water levels in the Sandhills are the products of interactions between rainfall, diffuse groundwater recharge, focused evaporation losses from lake surfaces, and surface drainage patterns [11]. At a regional scale, the water table follows the surface terrain but shows significant differences near lakes at local scales [41]. Locally, a lake can gain or lose water based on the position of the lake in relation to the regional groundwater flow regime and the gradient between the regional and local head [11]. A transient groundwater mound forms when lakes are closely spaced on a hummocky topography. The presence of groundwater mounds drives groundwater flow towards the lakes, whereas their absence causes the water to flow away from the lakes, resulting in changes in lake water levels [41]. In addition, seasonal changes in groundwater configuration also alter the location, magnitude, and direction of groundwater flow into or out of the lake [42].

Previous studies have demonstrated the potential of satellite altimetry for monitoring inland water levels (e.g., lakes, wetlands, and groundwater-dependent ecosystems) at centimeter-level accuracy when compared with in situ observations. Nevertheless, they have not been applied to infer groundwater levels of an unconfined aquifer using lake water levels. Our validation result indicates that the satellite altimetry provides close estimates of groundwater levels near densely populated lakes in the Sandhills. Our uncertainty estimates (0.68–0.75 m RMSE $\pm$ 0.45–0.76 m SD) between the individual lakes and observation wells observation closely correspond to standard error estimates of 0–1 m SE [14,43]. Although many observations would provide better estimates of regional groundwater level variability, only a limited number of observation wells were underlying unconfined aquifers near lakes and matched observations with ICESat-2 and SWOT. In addition, the accuracy of the water level depends on satellite attributes of a given satellite, such as observation

coverage, orbital characteristics, and sampling methods. The accuracy of SWOT depends on the variations in radar backscatter complexity, effective resolution, and incidence angle. Smaller incidence angles have higher accuracy, while larger incidence angles result in greater uncertainties [7,44]. Similarly, complex radar backscatters due to vegetation and ice layers on uneven lake surfaces contain multiple reflection points, leading to inaccurate distance measurements [8]. Although ICESat-2 results in higher vertical accuracy, its observations are affected by solar background noise, the ranging precision of the instrument, radial orbital uncertainty, forward scattering in the atmosphere, and tropospheric path delay uncertainty. The ranging precision is a function of the laser pulse width, the surface area illuminated by the laser, and uncertainty in the timing electronics [45]. Lake water levels are also affected by the uncertainty associated with the datums used. Although we transformed our data into NAVD and NAD83 (2011) datums, datum transformation and errors associated with the datums result in some uncertainty in the lake water level estimates [8]. Despite these limitations, the ability of ICESat-2 and SWOT to image large areas of the Sandhills at higher spatial and temporal coverage is an exceptional opportunity to characterize regional groundwater dynamics.

Groundwater levels in the Sandhills represent complex hydrogeological and environmental factors. Geostatistics, namely kriging and its variants using the spatial structure of variables, frequently yields the most unbiased estimates and enables quantification of estimation errors [37]. However, the reliability of the predicted unsampled locations is influenced by several sources of uncertainty, such as measurement error, spatial distribution of the sample points, selection and parameterization of the semivariogram. Our study showed that well-distributed sample points within a study area result in less standard error and, therefore, less uncertainty. In contrast, a clumped distribution of sample points produces higher error and uncertainty. Our interpolated surface using GAM outperformed KED when predicting groundwater levels in the Sandhills. KED generated a smoother error surface throughout the Sandhills, while GAMs inherently capturing local nonlinearities resulted in lower error in interdunal lakes and wetlands while higher error in areas with sand dunes. GAMs have produced better estimates where a nonlinear relationship exists between the predictor and response variables [19]. However, GAM's predictive capability relies on careful selection and characterization of a smoothing function, which is typically complicated and needs parametrization for every other model. Our study, considering replicability and computation cost, only used surface topography to remove the regionalized trend and capture the local variation in the groundwater level [14,38]. However, groundwater levels in the Sandhills are a function of other hydrogeological variables such as depth to water, thickness and geologic composition of the unsaturated zone, and hydraulic characteristics of the aquifer [46].

Our work demonstrates that satellite altimetry is a potential alternative for the monthly measurement of LGL in the Nebraska Sandhills. Such monthly measurements facilitate improved understanding and prediction of groundwater flooding in remote areas [3,47], which may impact many human activities such as the transit of the few throughgoing, paved roads in a sparsely populated area like the Sandhills (Figure S3). We intend to imply that our method is not a perfect solution to evaluate groundwater level variation at a monthly scale. In fact, we propose it as one of the many potential methods that can be employed to understand the general trend and pattern of groundwater level variation at the landscape scale. Furthermore, we speculate that new satellite missions, advanced processing algorithms, integration with ground-based sensors (potentially including, e.g., time-lapse imagery [48]), and improved cyberinfrastructure may eventually enable the quarterly or weekly measurement of groundwater levels in the Sandhills. Satellite altimetry could also be applied to groundwater-level measurements in geologically and hydrolog-

ically similar regions worldwide. Potential regions of application include the Badain Jaran Desert in western Inner Mongolia in China, glaciated parts of Europe, southeastern Australia, the East African Rift in Kenya and Ethiopia, and others [49–53].

## 5. Limitations and Future Work

Although the proposed framework demonstrates the potential of satellite altimetry to measure the groundwater level, multiple limitations and sources of uncertainty must be taken into account: (1) The measurement uncertainties of satellite altimetry may propagate to the groundwater estimates. (2) Considering the uncertainty stemming from the use of fewer observation wells for the validation of lake groundwater level, future studies should incorporate a larger number of observations. (3) Although our study used topographic elevation as a covariate, interpolation using additional environmental covariates could provide better estimates of groundwater-level variation and its uncertainties. (4) Our study using four months to demonstrate the feasibility may not represent the seasonal, long-term, and extreme climate conditions, but future studies should use longer months and years. (5) In our method, it is assumed that lake levels adequately represent groundwater levels. Therefore, future studies should evaluate the effect of the overall environment on lake water levels and groundwater discharge.

## 6. Conclusions

Our research demonstrates that satellite altimetry enables us to measure groundwater level using lake water level in the Nebraska Sandhills. The results indicate that such an approach provides a viable alternative in regions where in situ groundwater monitoring is sparse or unevenly distributed. Uncertainties arising from measurement errors, spatial interpolation, and model assumptions must be considered for decision-making purposes. More specifically, measurements at monthly frequency using current technologies may provide insights into trends and patterns but are likely to have overlapping uncertainties. However, with the continued advancement of satellite missions, improved data processing algorithms, and enhanced computational infrastructure, satellite altimetry is expected to enable groundwater monitoring at unprecedented spatial and temporal scales. Overall, the integration of satellite altimetry with interpolation methods offers a promising approach for improving regional-scale groundwater assessments.

**Supplementary Materials:** The following supporting information can be downloaded at https://www.mdpi.com/article/10.3390/w18131601/s1, Table S1: ICESat-2 LGL (lake groundwater level) validation with corresponding date and time (time not shown here) of observation wells. The calculated MSE, RMSE, and SD corrected for ambient hydraulic gradient are shown at the end of table; Table S2: SWOT LGL (lake groundwater level) validation with corresponding date and time (time not shown here) of observation wells. The calculated MSE, RMSE, and SD corrected for ambient hydraulic gradient are shown at the end of table; Table S3: Comparison between GAM models for the corresponding months. Inclusion on terrain elevation as smooth parameter although resulted in lower error, resulted in higher standard deviation in prediction; Table S4: Parameters for GAM models used for May, June, July, and August of 2023; Figure S1: A comparison between variogram models for the months of May, June, July, and August of 2023. Left panels show semivariogram while the right panels show the directional semivariogram models for respective months; Figure S2: Residual histogram and Q-Q plots for the months of May (a,b), June (c,d), July (e,f), and August (g,h) of 2023; Figure S3: Comparison between contours generated using KED and GAMs. Both methods capture the general trend while the differences lie in the area with sparse LGL observations; Figure S4: Picture takes in September 2019 showing groundwater flooding in highways of Nebraska Sandhills after March 2019 flooding.

**Author Contributions:** Conceptualization, N.S.; methodology, N.S.; validation, N.S.; formal analysis, N.S.; investigating, N.S., T.E.G., A.R.M. and R.M.J.; resources, N.S., T.E.G., A.R.M. and R.M.J.; writing—original draft, N.S.; writing—review and editing, N.S., T.E.G., A.R.M. and R.M.J.; project administration, N.S.; funding acquisition, N.S., T.E.G., A.R.M. and R.M.J. All authors have read and agreed to the published version of the manuscript.

**Funding:** This research was funded by the U.S. Geological Society (USGS) Water Resources Research Act through the USGS 104(b) program award number (G21AP10612-05).

**Data Availability Statement:** The ICESat-2 ATL08 data used in the study are available at the National Snow and Ice Datacenter (NSIDC) via https://doi.org/10.5067/ATLAS/ATL08.007 (accessed on 14 May 2026) [30]. The SWOT Level 2 Lake Single-Pass Vector Data Product, Version D, is available via https://doi.org/10.5067/SWOT-LAKESP-D (accessed on 14 May 2026) [32]. The water level data from observation wells are available via "https://snr.unl.edu/data/water/groundwater/realtime/default.aspx (accessed on 5 March 2026)". The validated water level data is available in the Supplementary Material. Further inquiries can be directed to the corresponding author.

**Acknowledgments:** We would like to thank the editors and anonymous reviewers for constructive suggestions and feedback.

**Conflicts of Interest:** The authors declare that they have no known competing financial interests or personal relationships that could have appeared to influence the work reported in this paper.

## References

1. Döll, P.; Hoffmann-Dobrev, H.; Portmann, F.T.; Siebert, S.; Eicker, A.; Rodell, M.; Strassberg, G.; Scanlon, B.R. Impact of Water Withdrawals from Groundwater and Surface Water on Continental Water Storage Variations. *J. Geodyn.* **2012**, *59–60*, 143–156. [CrossRef]
2. Singh, A.; Mishra, S.; Ruskauff, G. Model Averaging Techniques for Quantifying Conceptual Model Uncertainty. *Ground Water* **2010**, *48*, 701–715. [CrossRef] [PubMed]
3. Mittelstet, A.R. *Groundwater Flooding on Highways in the Nebraska Sandhills: Applying Remote Sensing, Precipitation and Groundwater Modeling to Determine Depth, Cause and Frequency*; Nebraska Department of Transportation: Lincoln, NE, USA, 2025.
4. Meixner, T.; Manning, A.H.; Stonestrom, D.A.; Allen, D.M.; Ajami, H.; Blasch, K.W.; Brookfield, A.E.; Castro, C.L.; Clark, J.F.; Gochis, D.J.; et al. Implications of Projected Climate Change for Groundwater Recharge in the Western United States. *J. Hydrol.* **2016**, *534*, 124–138. [CrossRef]
5. Lall, U.; Josset, L.; Russo, T. A Snapshot of the World's Groundwater Challenges. *Annu. Rev. Environ. Resour.* **2020**, *45*, 171–194. [CrossRef]
6. Nielsen, K.; Stenseng, L.; Andersen, O.B.; Knudsen, P. The Performance and Potentials of the CryoSat-2 SAR and SARIn Modes for Lake Level Estimation. *Water* **2017**, *9*, 374. [CrossRef]
7. Fjørtoft, R.; Gaudin, J.-M.; Pourthié, N.; Lalaurie, J.-C.; Mallet, A.; Nouvel, J.-F.; Martinot-Lagarde, J.; Oriot, H.; Borderies, P.; Ruiz, C.; et al. KaRIn on SWOT: Characteristics of Near-Nadir Ka-Band Interferometric SAR Imagery. *IEEE Trans. Geosci. Remote Sens.* **2014**, *52*, 2172–2185. [CrossRef]
8. Wu, S.; Cai, Y.; Ke, C.-Q.; Xiao, Y.; Li, H.; He, Z.; Duan, Z. SWOT Mission Enables High-Precision and Wide-Coverage Lake Water Levels Monitoring on the Tibetan Plateau. *J. Hydrol. Reg. Stud.* **2025**, *59*, 102357. [CrossRef]
9. Köhn, S.J.; Nielsen, K. Evaluation of SWOT HR PIXC Version D Water Level Time Series of Small Lakes. *EGUsphere* **2026**, *2026*, 1–22. [CrossRef]
10. Biancamaria, S.; Lettenmaier, D.P.; Pavelsky, T.M. The SWOT Mission and Its Capabilities for Land Hydrology. In *Remote Sensing and Water Resources*; Cazenave, A., Champollion, N., Benveniste, J., Chen, J., Eds.; Springer International Publishing: Cham, Switzerland, 2016; pp. 117–147.
11. Zlotnik, V.A.; Olaguera, F.; Ong, J.B. An Approach to Assessment of Flow Regimes of Groundwater-Dominated Lakes in Arid Environments. *J. Hydrol.* **2009**, *371*, 22–30. [CrossRef]
12. Shrestha, N.; Mittelstet, A.R.; Gilmore, T.E.; Zlotnik, V.; Neale, C.M. Effects of Drought on Groundwater-Fed Lake Areas in the Nebraska Sand Hills. *J. Hydrol. Reg. Stud.* **2021**, *36*, 100877. [CrossRef]
13. Adane, Z.; Zlotnik, V.A.; Rossman, N.R.; Wang, T.; Nasta, P. Sensitivity of Potential Groundwater Recharge to Projected Climate Change Scenarios: A Site-Specific Study in the Nebraska Sand Hills, USA. *Water* **2019**, *11*, 950. [CrossRef]
14. Shrestha, N.; Mittelstet, A.R.; Young, A.R.; Gilmore, T.E.; Gosselin, D.C.; Qi, Y.; Zeyrek, C. Groundwater Level Assessment and Prediction in the Nebraska Sand Hills Using LIDAR-Derived Lake Water Level. *J. Hydrol.* **2021**, *600*, 126582. [CrossRef]

15. Adhikary, P.P.; Dash, C.J. Comparison of Deterministic and Stochastic Methods to Predict Spatial Variation of Groundwater Depth. *Appl. Water Sci.* **2017**, *7*, 339–348. [CrossRef]
16. Boezio, M.N.M.; Costa, J.F.C.L.; Koppe, J.C. Kriging with an External Drift versus Collocated Cokriging for Water Table Mapping. *Trans. Inst. Min. Metall. Sect. B Appl. Earth Sci.* **2006**, *115*, 103–112. [CrossRef]
17. Varouchakis, E.A.; Hristopulos, D.T. Comparison of Stochastic and Deterministic Methods for Mapping Groundwater Level Spatial Variability in Sparsely Monitored Basins. *Environ. Monit. Assess.* **2013**, *185*, 1–19. [CrossRef] [PubMed]
18. Kammann, E.E.; Wand, M.P. Geoadditive Models. *J. R. Stat. Soc. Ser. C Appl. Stat.* **2003**, *52*, 1–18. [CrossRef]
19. Aalto, J.; Pirinen, P.; Heikkinen, J.; Venäläinen, A. Spatial Interpolation of Monthly Climate Data for Finland: Comparing the Performance of Kriging and Generalized Additive Models. *Theor. Appl. Clim.* **2013**, *112*, 99–111. [CrossRef]
20. Feher, L.C.; Osland, M.J.; Johnson, D.J.; Grace, J.B.; Guntenspergen, G.R.; Stewart, D.R.; Coronado-Molina, C.; Sklar, F.H. Nonlinear Patterns of Surface Elevation Change in Coastal Wetlands: The Value of Generalized Additive Models for Quantifying Rates of Change. *Estuaries Coasts* **2024**, *47*, 1893–1902. [CrossRef]
21. Halperin, J.; LeMay, V.; Coops, N.; Verchot, L.; Marshall, P.; Lochhead, K. Canopy Cover Estimation in Miombo Woodlands of Zambia: Comparison of Landsat 8 OLI versus RapidEye Imagery Using Parametric, Nonparametric, and Semiparametric Methods. *Remote Sens. Environ.* **2016**, *179*, 170–182. [CrossRef]
22. Asquith, W.H.; Seanor, R.C.; McGuire, V.L.; Kress, W.H. Methods to Quality Assure, Plot, Summarize, Interpolate, and Extend Groundwater-Level Information—Examples for the Mississippi River Valley Alluvial Aquifer. *Environ. Model. Softw.* **2020**, *134*, 104758. [CrossRef]
23. Young, A.R.; Burbach, M.E.; Lackey, S.O.; Joeckel, M.R.; Westrop, J.P. *Nebraska Statewide Groundwater-Level Monitoring Report 2025*; University of Nebraska-Lincoln, Conservation and Survey Division: Lincoln, NE, USA, 2025; p. 24.
24. Loope, D.; Swinehart, J. Thinking Like a Dune Field: Geologic History in the Nebraska Sand Hills. *Gt. Plains Res. A J. Nat. Soc. Sci.* **2000**, *10*, 5–35.
25. Dappen, P.; Merchant, J.; Ratcliffe, I.; Robbins, C. *Delineation of 2005 Land Use Patterns for the State of Nebraska*; Center for Advanced Land Management Information Technologies, School of Natural Resources, University of Nebraska-Lincoln: Lincoln, NE, USA, 2007.
26. Sweeney, M.R.; Loope, D.B. Holocene Dune-Sourced Alluvial Fans in the Nebraska Sand Hills. *Geomorphology* **2001**, *38*, 31–46. [CrossRef]
27. Rossman, N.R.; Zlotnik, V.A.; Rowe, C.M. An Approach to Hydrogeological Modeling of a Large System of Groundwater-Fed Lakes and Wetlands in the Nebraska Sand Hills, USA. *Hydrogeol. J.* **2018**, *26*, 881–897. [CrossRef]
28. Gosselin, D.C.; Rundquist, D.C.; McFeeters, S.K. Remote Monitoring of Selected Ground-Water Dominated Lakes in the Nebraska Sand Hills. *J. Am. Water Resour. Assoc.* **2000**, *36*, 1039–1051. [CrossRef]
29. Szilagyi, J.; Zlotnik, V.A.; Gates, J.B.; Jozsa, J. Mapping Mean Annual Groundwater Recharge in the Nebraska Sand Hills, USA. *Hydrogeol. J.* **2011**, *19*, 1503–1513. [CrossRef]
30. Copernicus, S. Copernicus Sentinel Data. Available online: https://sentiwiki.copernicus.eu/web/s2-processing (accessed on 14 April 2026).
31. Neuenschwander, A.; Pitts, K.; Jelley, B.; Robbins, J.; Markel, J.; Popescu, S.; Nelson, R.; Harding, D.; Pederson, D.; Klotz, B.; et al. *ATLAS/ICESat-2 L3A Land and Vegetation Height*; Version 7; NASA National Snow and Ice Data Center Distributed Active Archive Center (NASA NSIDC DAAC): Boulder, CO, USA, 2025.
32. Fu, L.-L.; Pavelsky, T.; Cretaux, J.-F.; Morrow, R.; Farrar, J.T.; Vaze, P.; Sengenes, P.; Vinogradova-Shiffer, N.; Sylvestre-Baron, A.; Picot, N.; et al. The Surface Water and Ocean Topography Mission: A Breakthrough in Radar Remote Sensing of the Ocean and Land Surface Water. *Geophys. Res. Lett.* **2024**, *51*, e2023GL107652. [CrossRef]
33. NASA/JPL/PO.DAAC. *SWOT SWOT Level 2 Lake Single-Pass Vector Data Product 2025*; NASA/JPL/PO.DAAC: Pasadena, CA, USA, 2025.
34. Tian, S.; Zhang, X.; Tian, J.; Sun, Q. Random Forest Classification of Wetland Landcovers from Multi-Sensor Data in the Arid Region of Xinjiang, China. *Remote Sens.* **2016**, *8*, 954. [CrossRef]
35. Wang, C.; Jia, M.; Chen, N.; Wang, W. Long-Term Surface Water Dynamics Analysis Based on Landsat Imagery and the Google Earth Engine Platform: A Case Study in the Middle Yangtze River Basin. *Remote Sens.* **2018**, *10*, 1635. [CrossRef]
36. Belgiu, M.; Drăguţ, L. Random Forest in Remote Sensing: A Review of Applications and Future Directions. *ISPRS J. Photogramm. Remote Sens.* **2016**, *114*, 24–31. [CrossRef]
37. Goovaerts, P. *Geostatistics for Natural Resources Evaluation*; Oxford University Press on Demand: Oxford, UK, 1997.
38. Desbarats, A.J.; Logan, C.E.; Hinton, M.J.; Sharpe, D.R. On the Kriging of Water Table Elevations Using Collateral Information from a Digital Elevation Model. *J. Hydrol.* **2002**, *255*, 25–38. [CrossRef]
39. Wood, S.N. Generalized Additive Models. *Annu. Rev. Stat. Its Appl.* **2025**, *12*, 497–526. [CrossRef]
40. Liu, D.; Wang, Z.; Zhang, B.; Song, K.; Li, X.; Li, J.; Li, F.; Duan, H. Spatial Distribution of Soil Organic Carbon and Analysis of Related Factors in Croplands of the Black Soil Region, Northeast China. *Agric. Ecosyst. Environ.* **2006**, *113*, 73–81. [CrossRef]

41. Winter, T.C. Relation of Streams, Lakes, and Wetlands to Groundwater Flow Systems. *Hydrogeol. J.* **1999**, *7*, 28–45. [CrossRef]
42. Winter, T.C. Effect of Ground-Water Recharge on Configuration of the Water Table beneath Sand Dunes and on Seepage in Lakes in the Sandhills of Nebraska, U.S.A. *J. Hydrol.* **1986**, *86*, 221–237. [CrossRef]
43. Sahoo, S.; Russo, T.A.; Elliott, J.; Foster, I. Machine Learning Algorithms for Modeling Groundwater Level Changes in Agricultural Regions of the U.S. *Water Resour. Res.* **2017**, *53*, 3878–3895. [CrossRef]
44. Zhang, Z.; Bo, Y.; Jin, S.; Chen, G.; Dong, Z. Dynamic Water Level Changes in Qinghai Lake from Integrating Refined ICESat-2 and GEDI Altimetry Data (2018–2021). *J. Hydrol.* **2023**, *617*, 129007. [CrossRef]
45. Neuenschwander, A.L.; Magruder, L.A. The Potential Impact of Vertical Sampling Uncertainty on ICESat-2/ATLAS Terrain and Canopy Height Retrievals for Multiple Ecosystems. *Remote Sens.* **2016**, *8*, 1039. [CrossRef]
46. Burbach, M.E.; Joeckel, R.M. A Delicate Balance: Rainfall and Groundwater in Nebraska during the 2000-2005 Drought. *Gt. Plains Res.* **2006**, *16*, 5–16.
47. Bundy, L.R.; Anderson, M.R.; Rowe, C.; Mahmood, R. Roadway Floods and Their Associated Weather-Related Conditions: New Insights Using CARS 511 Data for State and Federal Highways in Nebraska, USA. *Transp. Res. Interdiscip. Perspect.* **2023**, *22*, 100955. [CrossRef]
48. Gilmore, T.E.; Chapman, K.W.; Harner, M.J.; Bajelan, J.; Terry, C.; Stranzl, J.E., Jr.; Mittelstet, A.R.; Chapman, C.D.; Mehrubeoglu, M. A New GRIME2: Using an Octagon Calibration Target and Trail Camera to Measure Stream Water Level Over a 2-Year Period. *Water Resour. Res.* **2026**, *62*, e2025WR042244. [CrossRef]
49. Byrne, A.; Norris, K.; Chadwick, M.A.; Avery, S.; Olaka, L.; Tebbs, E.J. Rising Lake Levels in Central East Africa Are Driven by Increasing Rainfall and Land-Use Intensification. *J. Hydrol. Reg. Stud.* **2024**, *56*, 101999. [CrossRef]
50. Chen, J.S.; Li, L.; Wang, J.Y.; Barry, D.A.; Sheng, X.F.; Gu, W.Z.; Zhao, X.; Chen, L. Groundwater Maintains Dune Landscape. *Nature* **2004**, *432*, 459–460. [CrossRef] [PubMed]
51. Darling, W.G.; Gizaw, B.; Arusei, M.K. Lake-Groundwater Relationships and Fluid-Rock Interaction in the East African Rift Valley: Isotopic Evidence. *J. Afr. Earth Sci.* **1996**, *22*, 423–431. [CrossRef]
52. Turner, J.V.; Townley, L.R. Determination of Groundwater Flow-through Regimes of Shallow Lakes and Wetlands from Numerical Analysis of Stable Isotope and Chloride Tracer Distribution Patterns. *J. Hydrol.* **2006**, *320*, 451–483. [CrossRef]
53. Yang, X.; Ma, N.; Dong, J.; Zhu, B.; Xu, B.; Ma, Z.; Liu, J. Recharge to the Inter-Dune Lakes and Holocene Climatic Changes in the Badain Jaran Desert, Western China. *Quat. Res.* **2010**, *73*, 10–19. [CrossRef]


**Disclaimer/Publisher's Note:** The statements, opinions and data contained in all publications are solely those of the individual author(s) and contributor(s) and not of MDPI and/or the editor(s). MDPI and/or the editor(s) disclaim responsibility for any injury to people or property resulting from any ideas, methods, instructions or products referred to in the content.